construction materials

MDPI

Article

Assessing the Effects of Activator Formulation on Hardened Properties of Alkali-Activated Slag Mortars Using Ultrasound Pulse Velocity (*UPV*) Technique

Victor M. E. Lima [1,*], Igor V. Fernandes [2], Diego H. Alves [1], Tiago M. S. Agra [2], Danilo J. da C. Barbosa [2], Eudes A. Rocha [1] and Antonio A. Melo Neto [2]

[1] Polytechnic School, University of Pernambuco, Rua Benfica 455, Recife 50720-001, Brazil; dhas@poli.br (D.H.A.); eudes.rocha@poli.br (E.A.R.)
[2] Laboratory of Binder Technology, Department of Civil and Environmental Engineering, Federal University of Pernambuco, LabTag, Recife 50740-550, Brazil; igor.vfernandes@ufpe.br (I.V.F.); tiago.agra@ufpe.br (T.M.S.A.); danilo.jbarbosa@ufpe.br (D.J.d.C.B.); antonio.meloneto@ufpe.br (A.A.M.N.)
* Correspondence: victor.estolano@upe.br

Abstract

The *UPV* technique has been widely employed to predict the hardened properties of Portland cement mixtures. This article assesses the hardened properties of alkali-activated blast furnace slag mortars by comparing *UPV* measurements with compressive strength and dry density and calculating the dynamic modulus of elasticity from *UPV* results. The mixtures were prepared varying the type of activator (sodium metasilicate and sodium silicate), the content of Na_2O in the activators (3.0, 4.5, 6.0, and 7.5%), and the water/binder ratio. The results showed that exponential models showed medium and high determination coefficients (R^2), which explained the correlation between *UPV* and hardened properties. It was observed a limitation on the measurements of *UPV*, which did not surpass 4.4 km/s, which made it difficult to predict compressive strength value above 50 MPa. The dynamic modulus of elasticity calculated from *UPV* showed reliable results, even varying the Poisson's coefficient between 0.15 and 0.25. Lastly, it was also observed that a correlation between the content of C-S-H and *UPV* suggested that this technique can also be used to predict the evolution of the hydration products in alkali-activated slag mixtures.

Keywords: ultrasound pulse velocity; alkali-activated slag; compressive strength; alkaline activator

check for updates

Received: 5 October 2025
Revised: 12 November 2025
Accepted: 14 November 2025
Published: 25 November 2025

Citation: Lima, V.M.E.; Fernandes, I.V.; Alves, D.H.; Agra, T.M.S.; Barbosa, D.J.d.C.; Rocha, E.A.; Melo Neto, A.A. Assessing the Effects of Activator Formulation on Hardened Properties of Alkali-Activated Slag Mortars Using Ultrasound Pulse Velocity (*UPV*) Technique. *Constr. Mater.* **2025**, *5*, 84. https://doi.org/10.3390/constrmater5040084

Copyright: © 2025 by the authors. Licensee MDPI, Basel, Switzerland. This article is an open access article distributed under the terms and conditions of the Creative Commons Attribution (CC BY) license (https://creativecommons.org/licenses/by/4.0/).

1. Introduction

The use of alkali-activated binders (AAB) has been extensively studied as an alternative to Portland cement (PC), since AAB can exhibit comparable mechanical performance and significantly lower greenhouse gas emissions [1,2]. Moreover, the practical application of AAB has increased in recent decades, despite several reported limitations, such as supply chain constraints, high shrinkage of the hardened material, and variations in slag composition, which remain barriers to large-scale implementation [3]. Additionally, there is still a gap in experimental data involving different types and concentrations of precursors and activators, particularly from non-destructive testing methods, whose data are readily available in the literature for Portland cement systems [4–10]. Therefore, further research is needed to provide comprehensive non-destructive testing data for AAB materials.

The use of non-destructive tests is an alternative to destructive techniques, especially for compressive strength and modulus of elasticity. Several non-destructive tests are

utilized, such as ultrasound, rebound hammer (sclerometer test), and thermography, in addition to other methods that are commonly used in civil construction [11].

The ultrasound test is a quick and friendly technique that instantly provides data on the pulse velocity (*UPV*) traveling through the specimen. With this data, it is possible to estimate concrete compressive strength and modulus of elasticity. Regarding the compressive strength (*S*), there are several ways to correlate this property with *UPV*. According to Trtnik et al. [12], the most popular formula that establishes this relationship is.

According to Trtnik et al. [12], the most popular formula that establishes this relationship is:

$$S = \alpha e^{\beta \times UPV} \quad (1)$$

where α and β are empirical parameters determined by the least squares method after the linearization of the model. In the study of Silva et al. [13], the exponential curve presented in Equation (1) presents a better fit compared to the exponential equation $f_c = \alpha \times UPV^{\beta}$.

On the other hand, Neville [4] states that there is no physical basis for correlating compressive strength and pulse velocity; however, as *UPV* relates to concrete density, an indirect and limited estimation can be performed to predict compressive strength. This limitation is also discussed in a study with recycled aggregate developed by Estolano et al. [14], who showed that compressive strength might not correlate with ultrasound parameters depending on the situation analyzed.

In this context, an adequate manner of employing an ultrasound test is to predict the dynamic modulus of elasticity ($E_{c,d}$), as this property is physically linked to density. The most used formula to predict the modulus of elasticity from *UPV* is

$$E_{c,d} = \rho \times (UPV)^2 \times \frac{(1+\mu)(1-2\mu)}{(1-\mu)} \quad (2)$$

where ρ is the density and μ is the Poisson's ratio of the specimen. This formula (Equation (2)) is widely employed by standards worldwide, such as ASTM C597 [15], EN 12504-4 [16], and ABNT NBR 15630 [17].

In alkali-activated binders, there are few research using ultrasound to predict hardened properties. Mahmood et al. [18] employed the ultrasound pulse velocity technique to study the early-age properties of alkali-activated slag-fly ash mixtures. The authors compared the values with calorimetry data and observed that the determination coefficient between cumulative heat and *UPV* was higher than 0.95, showing a strong correlation. However, it was impossible to measure any pulse velocity in the first 24 h owing to the natural limitation of the equipment. In another study employing only blast furnace slag, Mahmood et al. [19] noticed that the high reaction rate associated with high silica modulus (Ms) of the activation solution allowed the identification of the increase in *UPV* on the first 24 h, which could not be identified in slag-fly ash mixtures. Assad et al. [20] studied the properties of metakaolin-slag alkali-activated mixtures at 180 and 360 curing days. In this paper, strong correlations were observed among *UPV*, compressive strength, and weight loss due to acid attack, and it was concluded that the mechanical behavior of the mortars increased as the slag content increased.

This article aims to evaluate the potential of ultrasound techniques for predicting the hardened properties of alkali-activated slag mixtures. The study seeks to address an existing gap in the literature, particularly concerning the relationship between ultrasonic parameters and the mechanical behavior of alkali-activated binders. Current standards are largely based on ordinary Portland cement systems, highlighting the need for further research to establish specific guidelines for alkali-activated materials. As the global use of these binders continues to expand, ongoing investigations are essential for developing a standardized framework for their characterization and assessment.

2. Materials and Methods

2.1. Materials

The precursor employed was blast furnace slag (BFS) to produce the alkali-activated mixtures. The BFS was characterized through chemical, physical, and mineralogical analyses to provide a better understanding of its properties. The chemical composition of BFS was assessed by XRF using a RIX 3000 Instrument (Rigaku, Tokyo, Japan). A D2 Phaser diffractometer (Bruker, Billerica, MA, USA) was employed to obtain the mineralogical characteristics of BFS. The parameters used in XRD were the following: 5–80° scan range, 0.02° angular step, 1.2°·min^{-1} scan speed, Cu-kα radiation with λ = 1.5406 Å, i = 10 mA and U = 30 kV. The qualitative analysis was conducted using the software Diffrac.EVA v.5.0 and the patterns from the ICDD database. Also, to complement the data of mineralogical and chemical characterization, thermogravimetric analysis (TGA) was performed through a thermobalance instrument (Mettler Toledo, Greifensee, Switzerland) in the temperature range of 30–1000 °C, heating rate of 10 °C·min^{-1}, and 40 mL·min^{-1} of N_2 rate. Finally, the physical characteristics of BFS were assessed by density test using the Le Chatelier flask, Blaine fineness, and particle size distribution through laser diffraction.

The activators used were pentahydrate sodium metasilicate (SMP) ($Na_2SiO_3 \cdot 5H_2O$) (Pernambuco Química, Jaboatão dos Guararapes, Brazil) and sodium silicate (SS) (Pernambuco Química, Jaboatão dos Guararapes, Brazil). SMP was provided as a solid and granular material, with silica modulus (Ms) (molar SiO_2/Na_2O ratio) = 1.01 and solid content = 57.56%. SS was acquired as a liquid solution with Ms = 1.75 and solid content = 45.25%.

The fine aggregate used to produce the mortars was quartz sand with the following parameters: maximum diameter size = 2.40 mm; fineness modulus = 2.00; d10 = 0.169 mm; d30 = 0.320 mm; d50 = 0.446 mm; d60 = 0.505 mm. According to these results, the aggregate was classified as fine well-graded sand.

2.2. Methods

2.2.1. Mix Design and Casting

The mixtures were prepared varying the concentration of Na_2O (%) of the alkaline activators, the type of activator, and the water/binder ratio, totaling 24 mixtures according to Table 1.

Table 1. Variables used in the experimental program.

Factors (1, 2, 3, 4 . . .)	Levels (A, B, C, D . . .)
1—Na_2O concentration (%)	A—3.0 B—4.5 C—6.0 D—7.5
2—Water/binder ratio	A—0.45 B—0.55 C—0.65
3—Type of activator	A—SMP B—SS
Total of mixtures	4 × 3 × 2 = 24

The proportioning of the blends followed other studies published in the literature [21–24]. The content of Na_2O (%), defined as one of the variables, was calculated following Equation (3):

$$Na_2O(\%) = \frac{Na_2O}{Na_2O + SiO_2 + BFS} \quad (3)$$

where Na_2O and SiO_2 are the masses of the respective components in the activators, and BFS is the mass of blast furnace slag. The sum of the denominator (Na_2O + SiO_2 + BFS) is the total mass of the binder in the mixtures; thus, in this research, the solids of the activators were also considered as binders.

After, the water/binder ratio was calculated according to Equation (4):

$$water/binder = \frac{w_{activator} + w_{additional}}{Na_2O + SiO_2 + BFS} \quad (4)$$

where $w_{activator}$ is the water already counted from the alkaline activator, and $w_{additional}$ is the added deionized water necessary to reach the target water/binder ratio.

Lastly, the proportion used to calculate the content of fine aggregate was 1:2 (total binder:sand).

The mixtures were formulated using a planetary mixer. Initially, 50% of the activator and the extra water were blended for 30 s. Concurrently, *BFS* was introduced into the mixture. Following an additional minute of mixing, the fine aggregate was incorporated, and mixing continued until reaching a total duration of 4 min and 30 s. The final step involved adding the remaining activator and continuing the mixing process for an additional minute, resulting in a cumulative mixing time of 5 min and 30 s.

To cast the specimens, cylindrical molds measuring 5 cm in diameter and 10 cm in height were employed. The mixtures were poured into four layers and compacted using a metallic rod with 30 strokes. Following demolding, the specimens were submerged in water for curing until they underwent hardened tests.

2.2.2. Testing

Ultrasound pulse velocity. Ultrasound tests were conducted using Pundit Lab equipment (Proceq, Schwarzenbach, Switzerland). The ultrasonic pulse transmission occurred at a frequency of 54 kHz and a width of 9.3 µs. The time the pulse travels across the specimen was calculated. With this time, the pulse speed (*UPV*) was obtained. The tests were conducted on cylindrical specimens, obtaining the pulse in the longitudinal direction. The conductive gel was employed to improve the electrical conductivity between the transducer and the specimen. Figure 1 shows the system assembled to measure *UPV*.

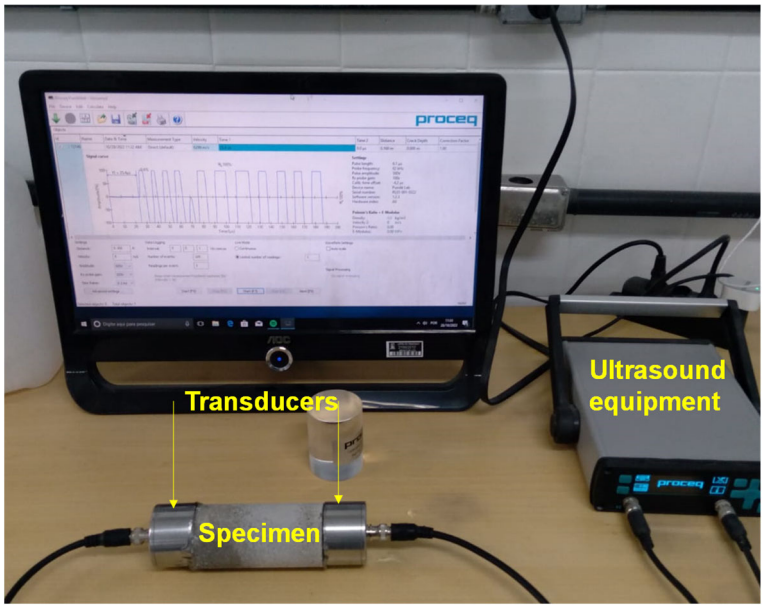


Figure 1. Apparatus to measure *UPV*.

To calculate the dynamic modulus of elasticity (E_{cd}), it is necessary to have the dry density (ρ) and Poisson's coefficient (μ) (Equation (3)). There are few investigations on Poisson's coefficient of alkali-activated materials, and the studies are generally conducted

in concrete and present a large variation in μ (0.13 to 0.22) [25–28]. Therefore, scenarios with μ varying from 0.15 to 0.25 were drawn for this study.

It is worth mentioning that the samples were tested in the saturated condition (saturated surface dry); that is, the analysis was carried out immediately after removing the specimen from the submerged curing, and it was slightly dried on its surface.

Compressive strength. The compressive strength test was performed in a AGX-V load machine (Shimadzu, Kyoto, Japan) with a load rate of 0.25 MPa/s for the cylindrical specimens according to ABNT NBR 7215 [29].

Dry density. The dry density test was obtained following the Brazilian standard ABNT NBR 9778 [30]. In this test, the specimens were subjected to saturation in water, and then the saturated mass (m_{sat}) and submerged (m_{sub}) in water were weighed using a hydrostatic balance. Then, the specimens were dried in an oven for 72 h, and the dry mass (msec) was obtained. The formula to calculate the dry density (d_{dry}) is:

$$d_{dry} = \frac{m_{sec}}{m_{sat} - m_{sub}} \quad (5)$$

Thermogravimetric analysis. A discussion was conducted using data from the thermogravimetric analysis. This test measured the continuous mass loss of pastes prepared with the same mix design of the mortars (except for the fine aggregate). This test was performed by a Mettler Toledo equipment, with a temperature range of 30–1000 °C, a heat rate of 10 °C·min^{-1}, and a purge N_2 gas equal to 45 mL·min^{-1}.

3. Results

3.1. Characterization of BFS

The chemical composition of BFS was assessed by X-ray fluorescence (XRF) and featured the presence of CaO (42.00%), SiO_2 (37.73%), Al_2O_3 (10.91%), MgO (6.04%), TiO_2 (0.52%), K_2O (0.46%), Na_2O (0.40%), and Fe_2O_3 (0.38%). The mineralogical composition evaluated through X-ray diffraction (XRD) showed the presence of 70.2% amorphous material, and the mineralogical phases observed were calcite, merwinite, and akermanite. The diffractogram of BFS, with identification of the mineralogical phases and their corresponding pattern codes, is presented in Figure 2.

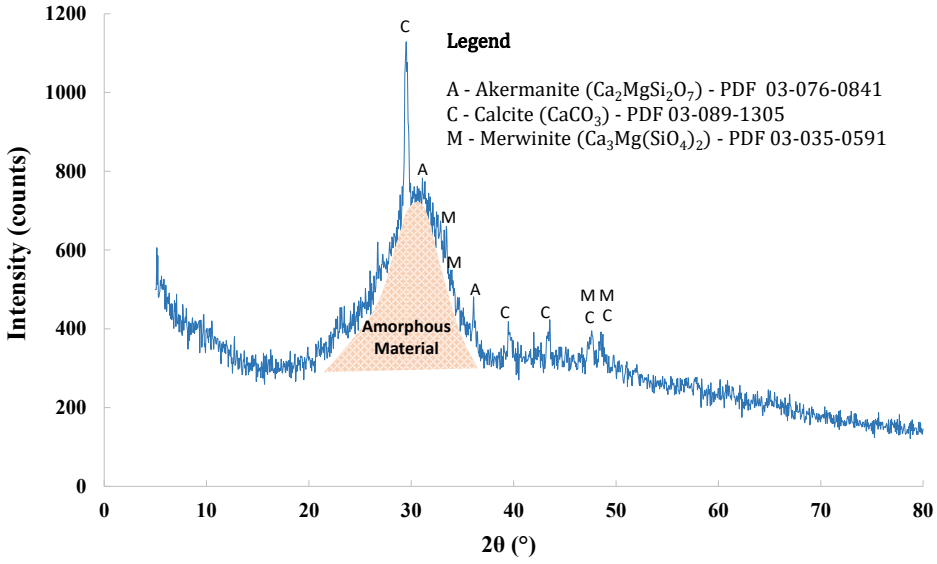


Figure 2. Diffractogram of BFS.

Figure 3 shows the result of thermogravimetric analysis (TGA) on BFS. As shown, a peak of mass loss at 50 °C appears owing to loss of humidity, and another remarkable peak at 665 °C, because of the decarbonation of calcite and poor crystalline phases of calcium carbonate. Concerning the physical characteristics of BFS, the results of tests were specific gravity = 2.79 g/cm^3; Blaine fineness = 442.2 m^2/kg; and the laser diffraction test provided a d_{50} value equal to 12.33 μm.

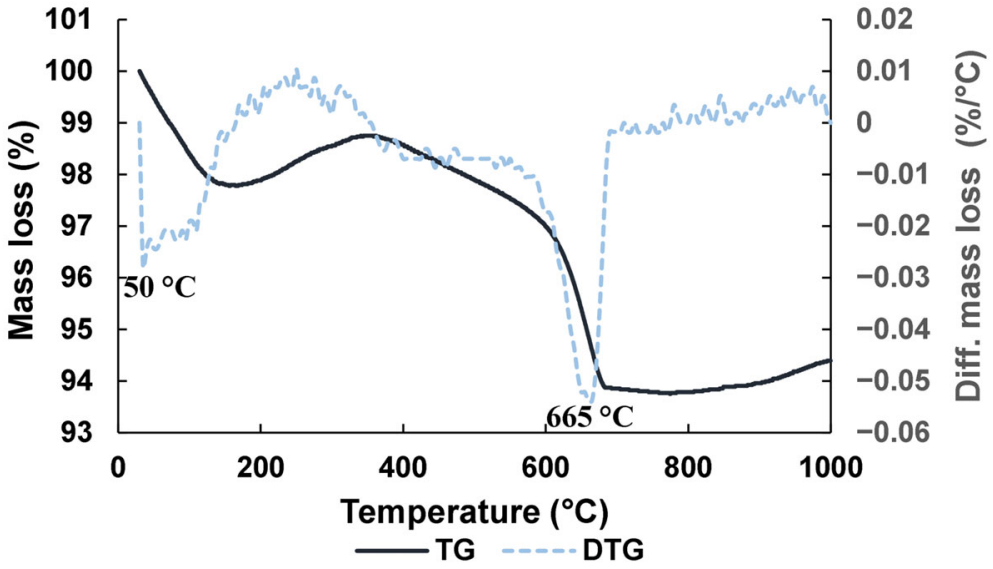


Figure 3. Result of TGA on BFS.

3.2. Ultrasonic Pulse Velocity

As observed in Figures 4 and 5, the *UPV* increased as the Na_2O content increased, which is attributed to the higher dissolution rate of the slag and the accelerated formation of C–(A)–S–H, leading to a denser microstructure and faster stiffness gain. Also, the influence of the water/binder ratio on *UPV* decreased as the water/binder ratio increased.

Toward the mixtures activated by SMP (Figure 4), the upper range value for *UPV* is 4.2 km/s. This value was reached by the mixtures with w/b = 0.45 and Na_2O dosages of 6.0 and 7.5%. This behavior agrees with microstructural data published in another paper [24], in which the high alkaline dosage accelerates the dissolution of BFS and, consequently, increases the hardening of the mixtures. Regarding the early ages, the influence of Na_2O (%) concentration of the alkaline activator is noticeable. The dosage of 7.5% Na_2O increased *UPV* at 3 days, which reached values close to 7 and 28 days, which suggests that high alkali dosages strongly accelerate the hardening at 3 days; however, at 28 days, *UPV* values are close between the dosages of 6.0% and 7.5%.

Similar conduct was found for the mixtures activated with SS (Figure 5). The samples reached a maximum of 4.4 km/s with the 7.5% Na_2O dosage. Especially with 4.5% Na_2O activator content, the velocities at 3 days are lower compared to mixtures with higher Na_2O content, but the results are close at 28 days for w/b = 0.45 and 0.55. The values at 28 days were very close, comparing the mixtures activated with 6.0 and 7.5% Na_2O (%), suggesting that the system reached a saturation point where the excess alkali did not further enhance hydration, and microcracking may have limited the final densification.

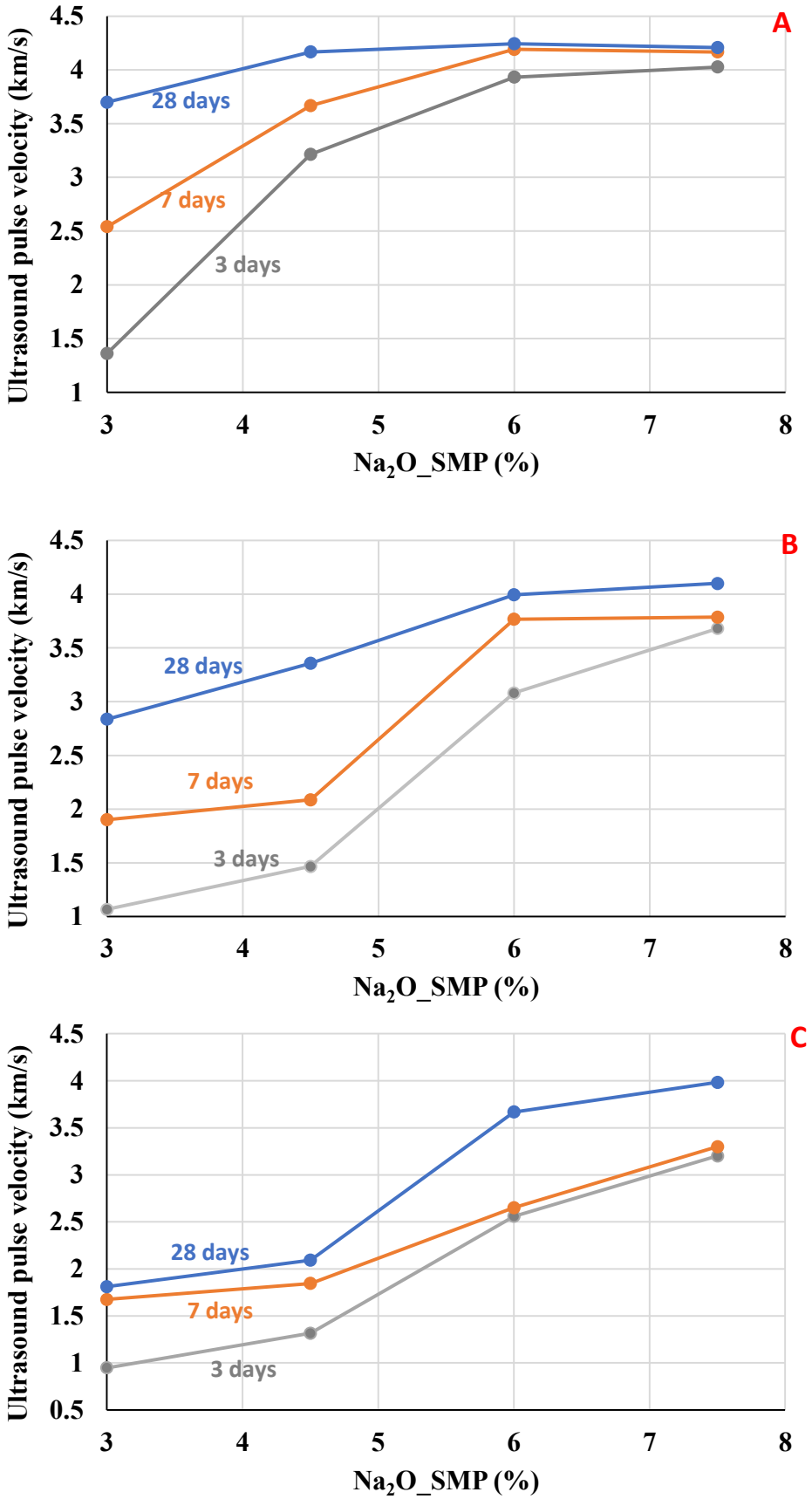


Figure 4. Ultrasound pulse velocities for mixtures activated with SMP with w/b = 0.45 (**A**), 0.55 (**B**), and 0.65 (**C**).

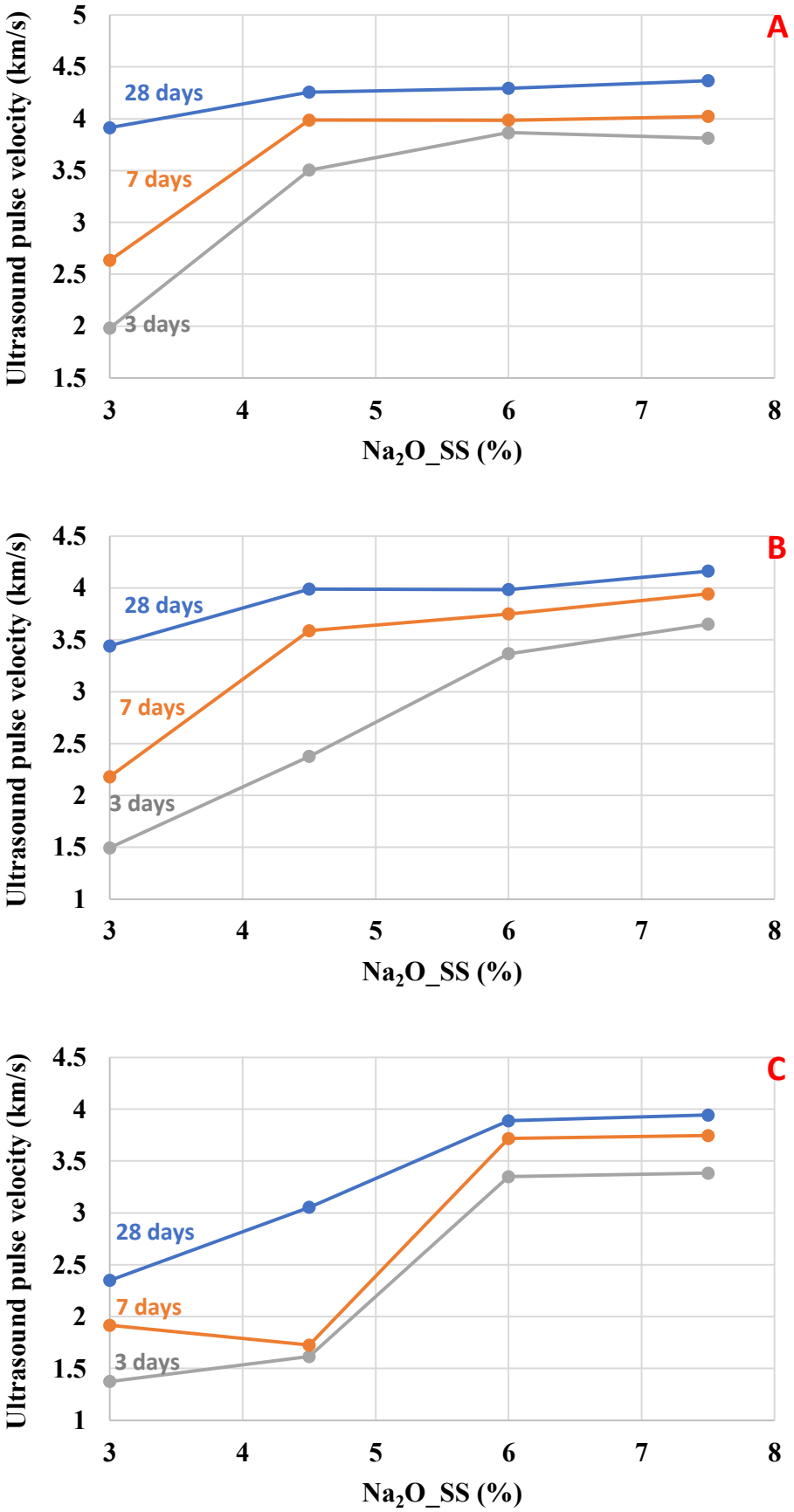


Figure 5. Results of ultrasound pulse velocity for mixtures activated by SS with w/b = 0.45 (**A**), 0.55 (**B**), and 0.65 (**C**).

3.3. Correlation with Compressive Strength

The compressive strength, *UPV*, and dry density results can be checked in this paper's Appendix A. The correlation between compressive strength and *UPV* is exposed in Figure 6. One of the questions raised by this paper concerns the ability of the ultrasound technique to predict the variations in the hardened properties caused by the difference in the alkali dosage of the activators. Figure 6 shows slight variations in compressive strength when the dosages of 6.0 and 7.5% were compared. Notwithstanding, it is possible to note the strength development due to the hydration reactions over time. Although limitations have been presented for the ultrasound test, Figure 6 shows an important correlation of this technique with compressive strength data.

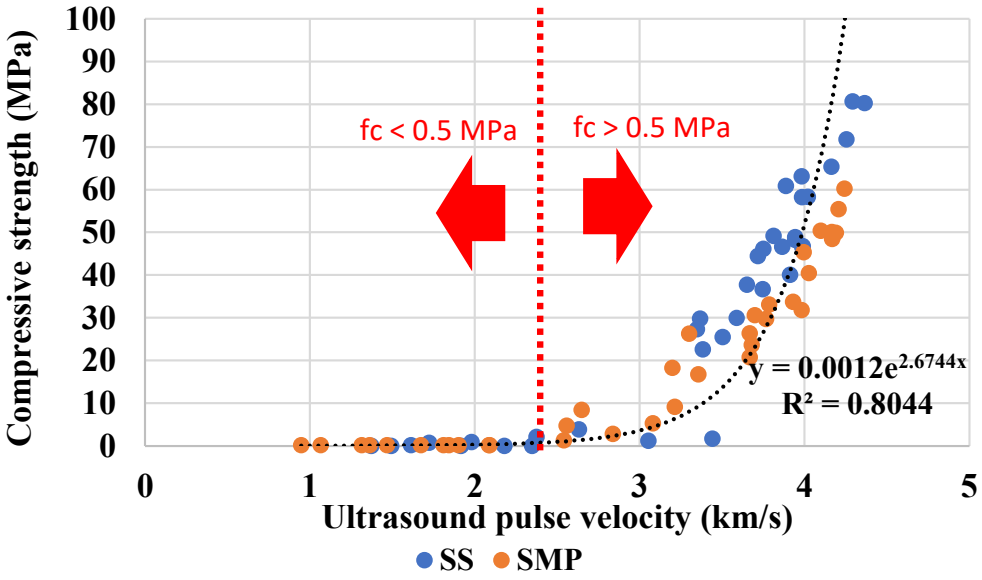


Figure 6. Scatter plot showing the correlation between ultrasound pulse velocity and compressive strength.

The exponential correlation reflects two distinct stages of material consolidation: a low-velocity regime dominated by early gel formation, and a high-velocity regime associated with significant strength development and matrix densification. Up to approximately 2.1 km/s, compression results are zero. Even if some hydration reactions occur and the specimen presents some rigidity, it is still insufficient to gain strength. On the other hand, samples with a velocity greater than 2.2 km/s begin to show significant compressive strength, and the curve tends to a steep straight line. It can also be observed that the samples activated with SMP presented slightly higher velocities for an equivalent resistance than the samples with SS.

The global equation with data of mixtures activated by SMP and SS was $f_c = 0.0012e^{2.6744UPV}$, according to Figure 4. Nevertheless, the samples activated by SMP and SS must be analyzed separately to predict the compressive strength more accurately. The equations found were $f_c = 0.0032e^{2.39UPV}$ ($R^2 = 0.92$) for mixtures with SMP and $f_c = 0.0021e^{2.55UPV}$ ($R^2 = 0.81$) for mixtures with SS. Analyzing the general equation (Equation (1)), in a study with concrete developed by Trtnik et al. [12], the coefficients of the equation were distant from the equations found by the authors, which were 0.0312 and 1.4896 for α and β, respectively. In another study with paste and concrete, Irrigaray et al. [7] found equations in the format $f_c = \alpha(UPV)^{\beta}$ and found the values of 3×10^{-14} and 4.2778 for α and β in the pastes, respectively, with $R^2 = 0.9766$. Compared to the mixtures of concretes, the determination coefficient of the correlation between *UPV* and compressive strength was higher when pastes were tested. Comparing this study with the literature is limited because the studies are usually conducted in concrete, which presents higher values for

UPV owing to the presence of coarse aggregate. It is also worth mentioning that most studies that delve into the study of ultrasound are conducted in Portland cement, as is the case with the articles cited in the current paragraph. Furthermore, those equations did not consider that, until a specific *UPV*, the compressive strength of the specimens is near zero. Therefore, in those studies, the extrapolation of the curves can lead to errors in the prediction of compressive strength.

Another possibility with the employment of the ultrasound is to provide rapid information about the range of compressive strength that the sample is inserted. This way, the predicted compressive strength values were sorted into ranges, as shown in Table 2. As previously stated, specimens with *UPV* below approximately 2.1 km/s show compressive strength near zero. On the other hand, there is a limitation to identifying compressive strengths above 50 MPa; thus, *UPV* values barely surpass 4.0 km/s.

Table 2. Predicted compressive strength (f_c) ranges from ultrasound pulse velocity (*UPV*) measurements.

Predicted Comp. Strength Range (MPa)	*UPV* Measured (km/s) (SMP)	*UPV* Measured (km/s) (SS)	*UPV* Measured (Global Equation)
<0.5	<2.11	<2.14	<2.12
0.5 < fc < 10	2.11 < *UPV* < 3.37	2.14 < *UPV* < 3.32	2.12 < *UPV* < 3.34
10 < fc < 20	3.37 < *UPV* < 3.66	3.32 < *UPV* < 3.59	3.34 < *UPV* < 3.62
20 < fc < 30	3.66 < *UPV* < 3.83	3.59 < *UPV* < 3.75	3.62 < *UPV* < 3.78
30 < fc < 40	3.83 < *UPV* < 3.95	3.75 < *UPV* < 3.86	3.78 < *UPV* < 3.90
40 < fc < 50	3.95 < *UPV* < 4.04	3.86 < *UPV* < 3.95	3.90 < *UPV* < 3.99
fc > 50	*UPV* > 4.04	*UPV* > 3.95	*UPV* > 3.99

3.4. Correlation with Dry Density

The correlation between dry density and *UPV* is shown in Figure 7. The global equation, including data of activation with SMP and SS, can be represented by an exponential relationship, with $\alpha = 1.6170$ and $\beta = 0.0472$, following the model of Equation (1). Separating the data between the types of activators used, the coefficients were $\alpha = 1.6591$ and $\beta = 0.0412$ for mortars activated by SMP, and $\alpha = 1.5127$ and $\beta = 0.0635$ for mixtures active with SS.

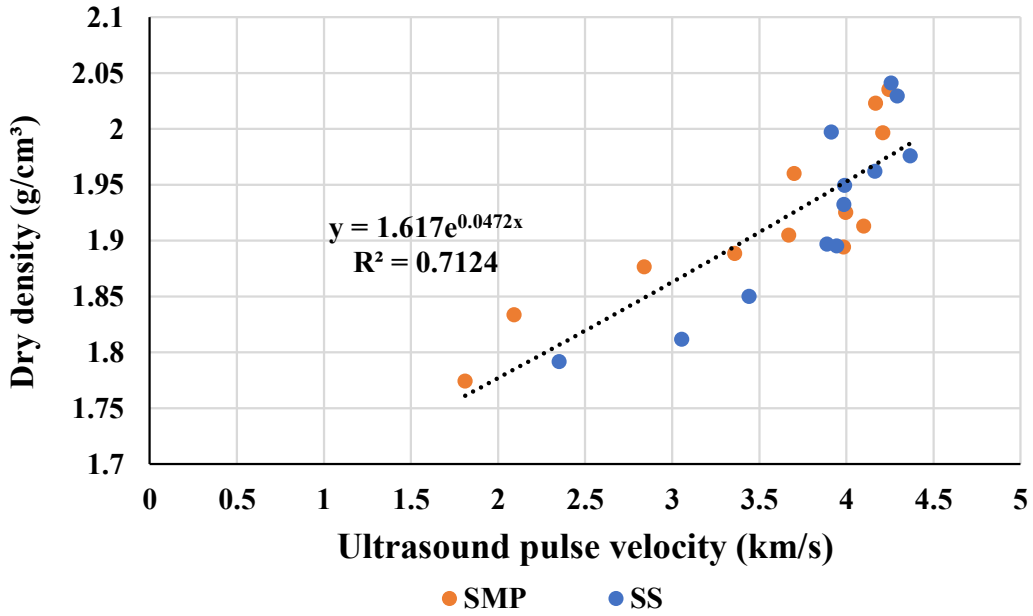


Figure 7. Correlation between ultrasound pulse velocity and dry density.

Results of non-destructive tests usually correlate with hardened density because the ultrasonic pulse takes longer as the porosity of the specimen increases [31]. Thereby, a high correlation between specimens is expected. Revilla–Cuesta et al. [32] found Pearson coefficients varying between 0.80 and 0.82, since the correlation between density and *UPV*. In another study with recycled aggregate, Estolano et al. [14] concluded that a linear equation can explain the correlation between dry density and dynamic modulus of elasticity with $R^2 = 0.94$.

Here, an exponential curve was chosen to explain the correlation between dry density and *UPV* following the same logic of Equation (1). However, the coefficient of determination (R^2) showed a medium correlation (0.70–0.80), and some reasons may explain this. First, as explained with the compressive strength results, the *UPV* technique shows some limitations in identifying cracks and microcracks caused by the excess of Na_2O dosage in the activators. Another possibility is the occurrence of gelling caused by the low silica modulus of SS, which the ultrasound may not capture. Even so, *UPV* can provide a reliable estimate to predict dry density.

3.5. Predicting Dynamic Modulus of Elasticity

To predict the dynamic modulus of elasticity ($E_{c,d}$), Equation (2) was utilized, varying the Poisson's coefficient among 0.15, 0.20, and 0.25. Figure 8 shows these results, where the data using $\mu = 0.20$ corresponds to the spots, and the predicted values with $\mu = 0.15$ and 0.25 correspond to the superior and inferior bars, respectively.

The maximum value found for the slag mixtures activated by SMP with w/b = 0.45 was obtained for the mixture with 6.0% Na_2O, which was 32.98 GPa, varying between 34.71 and 30.54 GPa, considering the variation in Poisson's ratio. However, for the other water/binder ratios, the mixtures with 7.5% Na_2O presented the highest values for dynamic modulus of elasticity, following the behavior of the compressive strength results. Concerning the mixtures activated with SS, the mixtures with 4.5, 6.0, and 7.5% presented similar values, which were 33.27, 33.65, and 33.90, respectively, considering $\mu = 0.20$ and w/b = 0.45. The influence of Na_2O is more pronounced in the w/b = 0.65, in which $E_{c,d}$ was only 8.89 GPa for Na_2O dosage = 3.0% and increased to 15.21 and 25.81 GPa when the Na_2O content increased to 4.5 and 6.0%, respectively.

Due to the difference in precursors, activators, and mix design methods, it is worth stating that the comparison among studies has several limitations. In a study with fly ash-based geopolymers, Alanazi et al. [33] found that the dynamic modulus of elasticity was about 20 GPa for mixtures with compressive strengths varying between 40 and 50 MPa. In the same article, mixtures with Portland cement with the same compressive strength range presented a modulus of elasticity surpassing 30 GPa. This occurred because the process of hardening of geopolymers is essentially by geopolymerization. On the other hand, in the alkali-activated slag mixtures, the formation of the C-(A)-S-H matrix occurs by geopolymerization and hydration [34], leading to stiffer mixtures with a higher modulus of elasticity compared to geopolymers. Thus, the behavior of the modulus of elasticity is similar between alkali-activated slag and ordinary Portland cement hardened blends. In the current paper, the modulus of elasticity varied between 25 and 33 GPa for mixtures with compressive strength in the range of 40–50 MPa, similar to the cement Portland mixtures of the referred study [33].

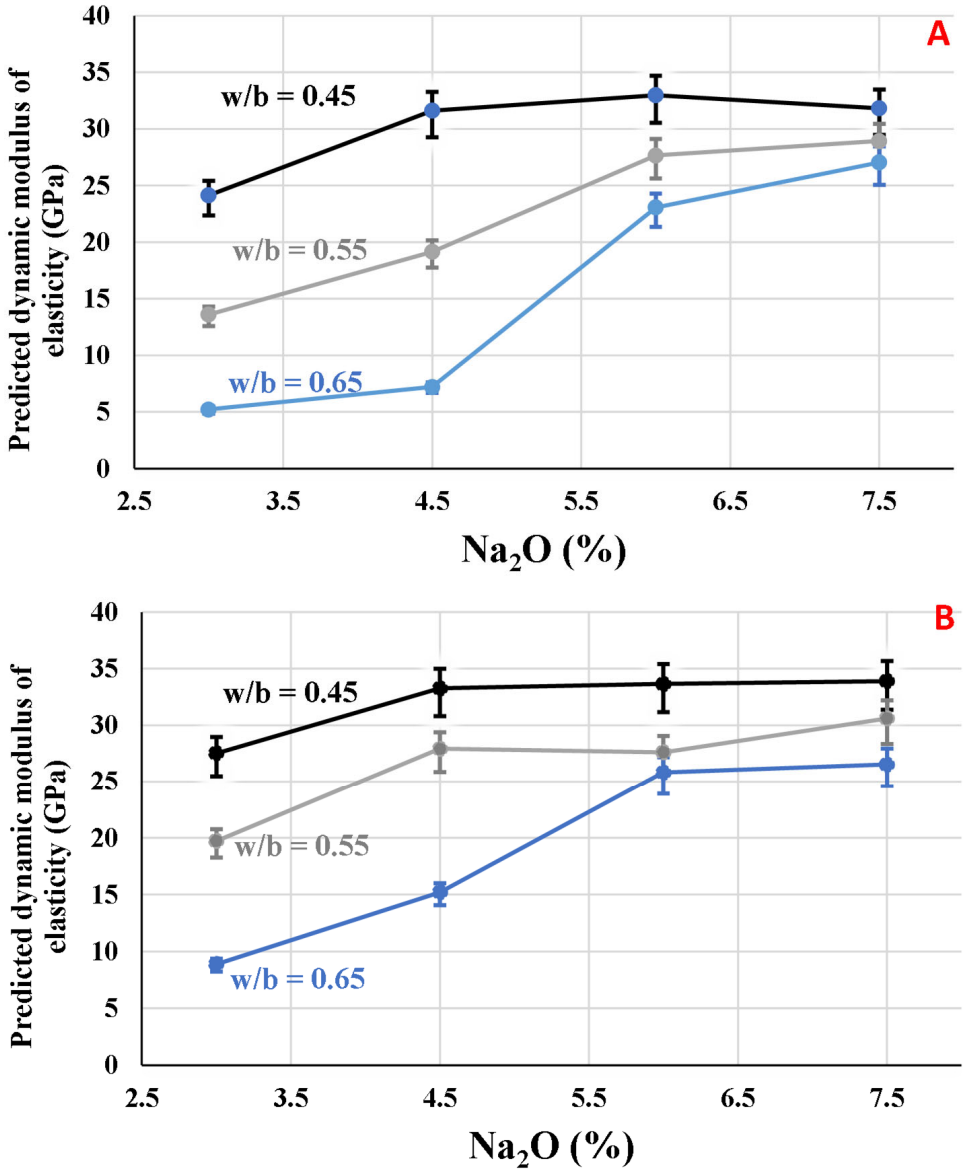


Figure 8. Results of predicted dynamic modulus of elasticity for slag mixtures activated by SMP (**A**) and SS (**B**). The spots represent the results with μ = 0.20; the superior and inferior bars show the results with μ = 0.15 and 0.25, respectively.

4. Discussion

In this study, the ultrasonic pulse velocity (*UPV*) technique was employed to predict the hardened properties of alkali-activated slag mixtures, following a similar rationale to that used for ordinary Portland cement systems. However, in the case of alkali activation, the analysis becomes more complex because several parameters influence the reaction kinetics and the final microstructure. These parameters can be defined either from an engineering dosage perspective or from chemical formulation variables. In the present research, the key parameter was the Na_2O content of the activator, which—as observed here and in other studies from the same doctoral project—strongly affects the dissolution rate of the slag and the subsequent hydration reactions, thereby controlling the hardening behavior of the mixtures.

Regarding the ultrasonic analysis, the results confirmed that *UPV* can effectively monitor the hardening evolution of alkali-activated slag mortars. An increase in *UPV* corresponds to a reduction in total porosity and to the progressive development of the elastic modulus and compressive strength. In alkali-activated slag systems, these im-

provements are intrinsically related to the formation of the C–(A)–S–H gel, which is the predominant hydration product, unlike geopolymers that typically form zeolitic and other aluminosilicate phases.

In this context, Figure 9 presents the relationship between *UPV* and the mass loss recorded between 50 and 200 °C in the thermogravimetric analysis, attributed to the release of physically bound water from the C–S–H structure. The figure shows a clear increasing trend in mass loss with increasing *UPV*, indicating that the ultrasonic response is sensitive to the rate of dissolution and precipitation processes that govern C–S–H formation. These processes occurred more intensively at Na_2O contents of 6.0 and 7.5%, where the reaction kinetics were accelerated. Therefore, *UPV* proved to be a reliable indirect indicator of hydration progress and microstructural refinement in alkali-activated slag mortars.

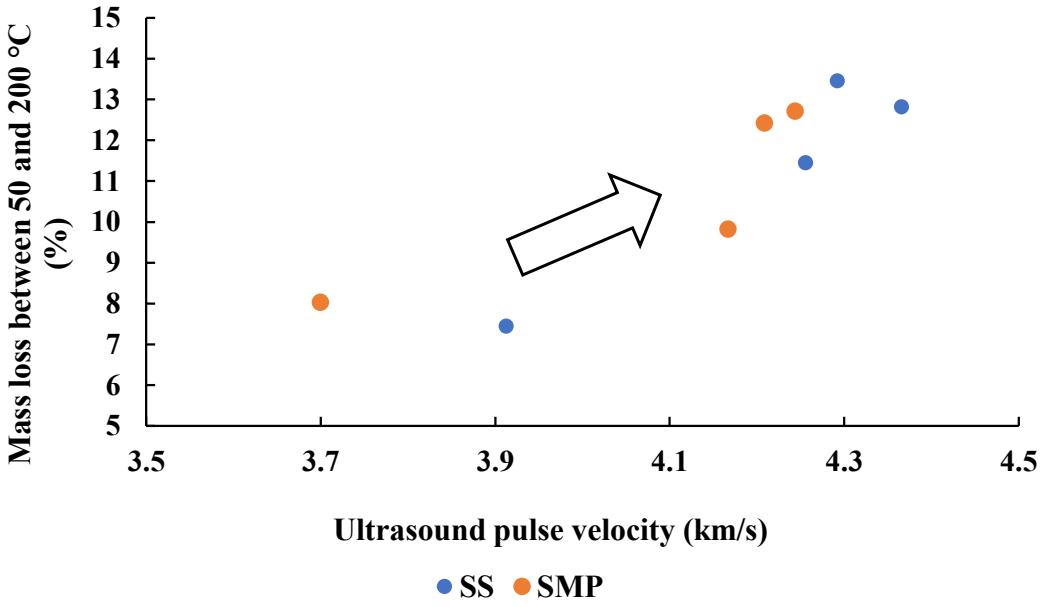


Figure 9. Relationship between *UPV* and mass loss between 50 and 200 °C from the thermogravimetric analysis.

Previous studies have already demonstrated the potential of ultrasound to monitor the hydration and early-age development of cementitious systems [18,19,35]. Nevertheless, further investigations are still required for alkali-activated binders, since their reaction mechanisms, gel composition, and microstructural evolution differ substantially from those of Portland cement-based materials.

5. Conclusions

This article aimed to use the *UPV* technique to predict the hardened properties of alkali-activated slag mixtures.

Mixtures with 3.0% Na_2O had the lowest *UPV* values due to the lack of sufficient alkalinity to activate the slag. From 4.5% Na_2O, a significant increase in *UPV* was observed compared to 3%, and it continued to increase less intensely until 6 and 7.5% Na_2O. The maximum limit in the *UPV* values was observed close to 6.0% Na_2O.

There was a medium R^2 to explain the relationship between dry density and *UPV*. This can be explained as this velocity is an outcome of the pulse that crosses the length of the sample, so it does not seem capable of identifying the voids caused by the high alkali content. The employment of a 7.5% Na_2O dosage led to a decrease in compressive strength and dry density compared to lower Na_2O contents.

The dynamic modulus of elasticity of alkali-activated mortars varied proportionally to *UPV* and compressive strength results. The mixtures obtained a maximum of 33.90 GPa for the mixture with 7.5% activated by SS and 32.98 for the mixture with 6.0% activated by SMP. Even varying the Poisson ratio between 0.15 and 0.25, small variations were observed, confirming that the interval shown was reliable in predicting the dynamic modulus of elasticity.

Lastly, it was noticed that these measurements from *UPV* correlated with chemical data from the thermogravimetric analysis regarding the estimation of C-S-H content. This indicates that the *UPV* technique can also be employed to assess the evolution of the reaction hydration of the mixtures.

The ultrasound test proved to be a useful tool in predicting compressive strength ranges. A limit was detected for compressive strength values above 50 MPa. Furthermore, it was found that the hardening of the material is achieved when the pulse speed is above approximately 2.15 km/s. Therefore, although the usefulness of the *UPV* technique in estimating hardened properties of alkali-activated slag mixtures, care must be taken when measuring high-strength mixtures (>50 MPa), as no significant differences can be observed from this strength level. To confirm this, a more detailed analysis is needed with the application of statistical tools to allow a reliable conclusion about the effectiveness of the use of ultrasound. Nevertheless, the findings indicate that *UPV* can also be applied as a non-destructive method for monitoring the hardening process and for quality control of alkali-activated slag mortars, providing a practical approach for both laboratory and field applications.

Author Contributions: Conceptualization, A.A.M.N.; Methodology, V.M.E.L.; Formal analysis, V.M.E.L.; Investigation, V.M.E.L., I.V.F. and D.J.d.C.B.; Resources, E.A.R.; Data curation, V.M.E.L., D.H.A. and T.M.S.A.; Writing—original draft, V.M.E.L. and D.J.d.C.B.; Writing—review & editing, I.V.F., D.H.A., T.M.S.A., E.A.R. and A.A.M.N.; Supervision, A.A.M.N.; Project administration, A.A.M.N. All authors have read and agreed to the published version of the manuscript.

Funding: This research was funded by Fundação de Amparo à Ciência e Tecnologia de Pernambuco (FACEPE), grant number BFD-0016-3.01/21 and Coordenação de Aperfeicoamento de Pessoal de Nível Superior (CAPES), grant number 88882.380324/2019-01.

Data Availability Statement: The original contributions presented in this study are included in the article. Further inquiries can be directed to the corresponding author.

Acknowledgments: The authors would like to thank the Brazilian agencies CAPES (Coordination for the Improvement of Higher Education Personnel) and FACEPE (Foundation for Supporting the Science and Technology of the State of Pernambuco) for their financial support. We also thank the companies Pernambuco Química S/A and Mizu Cimentos S/A for providing the materials for this research.

Conflicts of Interest: The authors declare no conflict of interest.

Appendix A

Table A1. Means of *UPV*, compressive strength, and dry density.

	Mix Design Features			Means of Results			
	Alkaline Activator	**Na_2O Dosage (%)**	**Water/Binder Ratio**	***UPV* (km/s)**	**Compressive Strength (MPa)**	**Dry Density (g/cm^3)**	**Mass Loss Between 50 and 100 °C (%)**
1	SMP	3.0	0.45	3.699	30.598	1.960	8.037
2	SMP	3.0	0.55	2.838	2.748	1.877	-
3	SMP	3.0	0.65	1.811	0.100	1.774	-

Table A1. *Cont.*

	Mix Design Features			Means of Results			
	Alkaline Activator	**Na_2O Dosage (%)**	**Water/Binder Ratio**	***UPV* (km/s)**	**Compressive Strength (MPa)**	**Dry Density (g/cm^3)**	**Mass Loss Between 50 and 100 °C (%)**
4	SMP	4.5	0.45	4.167	50.013	2.023	9.828
5	SMP	4.5	0.55	3.358	16.689	1.888	-
6	SMP	4.5	0.65	2.091	0.100	1.834	-
7	SMP	6.0	0.45	4.244	60.217	2.035	12.720
8	SMP	6.0	0.55	3.995	45.306	1.925	-
9	SMP	6.0	0.65	3.668	20.730	1.905	-
10	SMP	7.5	0.45	4.208	55.378	1.997	12.428
11	SMP	7.5	0.55	4.100	50.368	1.913	-
12	SMP	7.5	0.65	3.984	31.761	1.894	-
13	SS	3.0	0.45	3.913	40.056	1.997	7.451
14	SS	3.0	0.55	3.441	1.647	1.850	-
15	SS	3.0	0.65	2.349	0.100	1.792	-
16	SS	4.5	0.45	4.256	71.763	2.041	11.455
17	SS	4.5	0.55	3.990	46.752	1.950	-
18	SS	4.5	0.65	3.054	1.180	1.812	-
19	SS	6.0	0.45	4.292	80.628	2.029	13.467
20	SS	6.0	0.55	3.984	63.075	1.932	-
21	SS	6.0	0.65	3.888	60.885	1.897	-
22	SS	7.5	0.45	4.366	80.214	1.976	12.830
23	SS	7.5	0.55	4.163	65.363	1.962	-
24	SS	7.5	0.65	3.944	48.161	1.895	-

References

1. Pan, J.; Feng, K.; Li, M.; Xing, W.; Deng, X.; Chao, C. Performance optimisation of alkali-activated slag ultra-low carbon concrete (AAS-ULCC) for shield tunnel segments by steel fibres. *J. Clean. Prod.* **2025**, *486*, 144236. [CrossRef]
2. van Deventer, J.S.J.; Provis, J.L.; Duxson, P.; Brice, D.G. Chemical Research and Climate Change as Drivers in the Commercial Adoption of Alkali Activated Materials. *Waste Biomass-Valorization* **2010**, *1*, 145–155. [CrossRef]
3. Awoyera, P.; Adesina, A. A critical review on application of alkali activated slag as a sustainable composite binder. *Case Stud. Constr. Mater.* **2019**, *11*, e00268. [CrossRef]
4. Neville, A.M. *Properties of Concrete*; Trans-Atlantic Publications, Inc.: Philadelphia, PA, USA, 2011.
5. Zhao, M.; Nie, Z.; Wang, K.; Liu, P.; Zhang, X. Nonlinear ultrasonic test of concrete cubes with induced crack. *Ultrasonics* **2019**, *97*, 1–10. [CrossRef]
6. Mohammed, T.U.; Mahmood, A.H. Effects of maximum aggregate size on *UPV* of brick aggregate concrete. *Ultrasonics* **2016**, *69*, 129–136. [CrossRef]
7. Irrigaray, M.A.P.; Pinto, R.C.d.A.; Padaratz, I.J. A new approach to estimate compressive strength of concrete by the *UPV* method. *Rev. IBRACON Estrut. Mater.* **2016**, *9*, 395–402. [CrossRef]
8. Espinosa, A.B.; Revilla-Cuesta, V.; Skaf, M.; Faleschini, F.; Ortega-López, V. Utility of Ultrasonic Pulse Velocity for Estimating the Overall Mechanical Behavior of Recycled Aggregate Self-Compacting Concrete. *Appl. Sci.* **2023**, *13*, 874. [CrossRef]
9. Zhang, F.; Pang, K.; Li, J.; Liu, Q.; Du, J.; Xiao, H.; Guo, B.; Zhang, J. Ultrasonic pulse velocity as a non-destructive measure for the projectile impact resistance of cementitious composites across a wide range of mix compositions. *J. Build. Eng.* **2024**, *94*, 109875. [CrossRef]
10. Roobankumar, R.; SenthilPandian, M. Investigating the correlation between ultrasonic pulse velocity and compressive strength in polyurethane foam concrete. *Sci. Rep.* **2025**, *15*, 23995. [CrossRef] [PubMed]
11. Bolborea, B.; Baera, C.; Dan, S.; Gruin, A.; Burduhos-Nergis, D.-D.; Vasile, V. Concrete Compressive Strength by Means of Ultrasonic Pulse Velocity and Moduli of Elasticity. *Materials* **2021**, *14*, 7018. [CrossRef]
12. Trtnik, G.; Kavčič, F.; Turk, G. Prediction of concrete strength using ultrasonic pulse velocity and artificial neural networks. *Ultrasonics* **2009**, *49*, 53–60. [CrossRef]
13. Silva, F.A.N.; Delgado, J.M.P.Q.; Cavalcanti, R.S.; Azevedo, A.C.; Guimarães, A.S.; Lima, A.G.B. Use of Nondestructive Testing of Ultrasound and Artificial Neural Networks to Estimate Compressive Strength of Concrete. *Buildings* **2021**, *11*, 44. [CrossRef]
14. Estolano, V.; Fucale, S.; Filho, J.O.V.; Gabriel, D.; Alencar, Y. Assessment of static and dynamic modulus of elasticity in concrete made with recycled aggregate from concrete precast rejects. *Matéria* **2018**, *23*, e11974. [CrossRef]

15. *ASTM C 597-02*; Pulse Velocity Through Concrete. American Society for Testing and Material: West Conshohocken, PA, USA, 2016; Volume 4, pp. 3–6.
16. *E 12504-4*; Testing Concrete in Structures—Part 4: Determination of Ultrasonic Pulse Velocity. European Committee for Standardization: Brussels, Belgium, 2021.
17. *ABNT NBR 15630*; Mortars Applied on Walls and Ceilings—Determination of Elasticity Modulus by the Ultrasonic Wave Propagation. Brazilian Association of Technical Standards: Rio de Janeiro, Brazil, 2022.
18. Mahmood, A.H.; Babaee, M.; Foster, S.J.; Castel, A. Capturing the early-age physicochemical transformations of alkali-activated fly ash and slag using ultrasonic pulse velocity technique. *Cem. Concr. Compos.* **2022**, *130*, 104529. [CrossRef]
19. Mahmood, A.H.; Babaee, M.; Foster, S.J.; Castel, A. Continuous Monitoring of the Early-Age Properties of Activated GGBFS with Alkaline Solutions of Different Concentrations. *J. Mater. Civ. Eng.* **2021**, *33*, 04021374. [CrossRef]
20. Asaad, M.A.; Huseien, G.F.; Memon, R.P.; Ghoshal, S.; Mohammadhosseini, H.; Alyousef, R. Enduring performance of alkali-activated mortars with metakaolin as granulated blast furnace slag replacement. *Case Stud. Constr. Mater.* **2022**, *16*, e00845. [CrossRef]
21. de Lima, V.M.E.; Barros, L.C.; Neto, A.A.D.M. Characterization of sugarcane bagasse ash (SBA) and its evaluation for use in alkali-activated slag mixtures. *Cerâmica* **2021**, *67*, 123–130. [CrossRef]
22. Neto, A.A.M.; Cincotto, M.A.; Repette, W. Drying and autogenous shrinkage of pastes and mortars with activated slag cement. *Cem. Concr. Res.* **2008**, *38*, 565–574. [CrossRef]
23. Júnior, N.T.A.; Lima, V.M.; Torres, S.M.; Basto, P.E.; Neto, A.A.M. Experimental investigation of mix design for high-strength alkali-activated slag concrete. *Constr. Build. Mater.* **2021**, *291*, 123387. [CrossRef]
24. Lima, V.M.; Basto, P.A.; Henrique, M.A.; Almeida, Y.M.B.; Neto, A.A.D.M. Optimizing the concentration of Na2O in alkaline activators to improve mechanical properties and reduce costs and CO_2 emissions in alkali-activated mixtures. *Constr. Build. Mater.* **2022**, *344*, 128185. [CrossRef]
25. Thomas, R.J.; Peethamparan, S. Alkali-activated concrete: Engineering properties and stress–strain behavior. *Constr. Build. Mater.* **2015**, *93*, 49–56. [CrossRef]
26. Li, Z.; Nedeljković, M.; Chen, B.; Ye, G. Mitigating the autogenous shrinkage of alkali-activated slag by metakaolin. *Cem. Concr. Res.* **2019**, *122*, 30–41. [CrossRef]
27. Hojati, M.; Radlińska, A. Shrinkage and strength development of alkali-activated fly ash-slag binary cements. *Constr. Build. Mater.* **2017**, *150*, 808–816. [CrossRef]
28. Sajan, P.; Jiang, T.; Lau, C.; Tan, G.; Ng, K. Combined effect of curing temperature, curing period and alkaline concentration on the mechanical properties of fly ash-based geopolymer. *Clean. Mater.* **2021**, *1*, 100002. [CrossRef]
29. *ABNT NBR 7215*; Portland Cement—Determination of the Compressive Strength. Brazilian Association of Technical Standards: Rio de Janeiro, Brazil, 2019.
30. *ABNT NBR 9778*; Hardened Mortar and Concrete—Determination of Water Absorption, Void Index and Density. Brazilian Association of Technical Standards: Rio de Janeiro, Brazil, 2009.
31. de Lima, V.M.E.; Fucale, S.; Estolano, A.M.L.; Berenguer, R.A.; Cabral, L.C.; Nascimento, H.C.B.D.; de Lima, N.B. Concrete precast rejects—Treatment, characterization, and application in new concrete as recycled aggregate. *Conjecturas* **2021**, *21*, 142–181. [CrossRef]
32. Revilla-Cuesta, V.; Shi, J.-Y.; Skaf, M.; Ortega-López, V.; Manso, J.M. Non-destructive density-corrected estimation of the elastic modulus of slag-cement self-compacting concrete containing recycled aggregate. *Dev. Built Environ.* **2022**, *12*, 100097. [CrossRef]
33. Alanazi, H.; Hu, J.; Kim, Y.-R. Effect of slag, silica fume, and metakaolin on properties and performance of alkali-activated fly ash cured at ambient temperature. *Constr. Build. Mater.* **2019**, *197*, 747–756. [CrossRef]
34. Herrmann, A.; Koenig, A.; Dehn, F. Structural concrete based on alkali-activated binders: Terminology, reaction mechanisms, mix designs and performance. *Struct. Concr.* **2018**, *19*, 918–929. [CrossRef]
35. Bressan, H.F.G. Estudo do Comportamento de Ondas Ultrassônicas no Monitoramento do Concreto em Idades Iniciais. Master's Thesis, Universidade Federal de Santa Catarina, Florianópolis, Brazil, 2019.

Disclaimer/Publisher's Note: The statements, opinions and data contained in all publications are solely those of the individual author(s) and contributor(s) and not of MDPI and/or the editor(s). MDPI and/or the editor(s) disclaim responsibility for any injury to people or property resulting from any ideas, methods, instructions or products referred to in the content.